



OPEN

Characterizing nano-scale electrocatalysis during partial oxidation of methane

SUBJECT AREAS:
FUEL CELLS
ELECTROCATALYSISDaehee Lee¹, Dongha Kim¹, Joosun Kim² & Jooho Moon¹Received
11 September 2013Accepted
14 January 2014Published
3 February 2014Correspondence and
requests for materials
should be addressed to
J.M. (jmoon@yonsei.
ac.kr) or J.K. (joosun@
kist.re.kr)¹Department of Materials Science and Engineering, Yonsei University, 50 Yonsei-ro Seodaemun-gu, Seoul 120-749, Republic of Korea, ²High-Temperature Energy Materials Research Center, Korea Institute of Science and Technology, Seoul 136-791, Republic of Korea.

Electrochemical analysis allows *in situ* characterization of solid oxide electrochemical cells (SOCs) under operating conditions. However, the SOCs that have been analyzed in this way have ill-defined or uncommon microstructures in terms of porosity and tortuosity. Therefore, the nano-scale characterization of SOCs with respect to three-phase boundaries has been hindered. We introduce novel *in situ* electrochemical analysis for SOCs that uses combined solid electrolyte potentiometry (SEP) and impedance measurements. This method is employed to investigate the oscillatory behavior of a porous Ni-yttria-stabilized zirconia (YSZ) anode during the partial oxidation of methane under ambient pressure at 800 °C. The cyclic oxidation and reduction of nickel induces the oscillatory behavior in the impedance and electrode potential. The *in situ* characterization of the nickel surface suggests that the oxidation of the nickel occurs predominantly at the two-phase boundaries, whereas the nickel at the three-phase boundaries remains in the metallic state during the cyclic redox reaction.

Electrocatalysts are of key importance in solid oxide electrochemical cells (SOCs), such as solid oxide fuel cells (SOFCs) and solid oxide electrolysis cells (SOECs). SOCs provide the most promising technology for clean, efficient fuel generation and electric power production from both conventional and renewable energy sources¹⁻⁷. The electrodes in SOCs, where the electrochemical reactions occur, should be carefully designed with regard to the electrocatalytic activity and ionic-electronic conductivity. The state-of-the-art electrodes are composites of ion-conducting, electron-conducting, and catalytically active materials in which electrocatalytically active sites (i.e., three-phase boundaries (3PBs)) are maximized^{8,9}. However, the current understanding of the reaction mechanisms on a nano-scale is limited because of the scarcity of suitable *in situ* techniques. Therefore, three-dimensional reconstruction of the electrodes and a well-defined model system has been adopted to characterize the microstructural features and the reaction activity as a function of the 3PB site density^{1,10-14}. Although these previous efforts have provided valuable information about the electrocatalysts, the nano-scale elementary processes of the electrocatalytic reactions have not been clearly elucidated.

Electrochemical analysis has been employed to elucidate the driving force and reaction kinetics of electrocatalytic reactions¹⁵. In general, conventional solid electrolyte potentiometry (SEP) and impedance spectroscopy allow insight into electrochemical reactions by measuring global overpotentials and interfacial resistances¹⁶⁻²⁰. However, it is difficult to clarify how local distributions of overpotentials and resistances are related to the microstructural changes of nano-scale chemical states²¹. In particular, the reaction mechanisms of electrocatalysis are very complex because of the dissociative adsorption of reactants that takes place concurrently with the electrochemical reactions. The electrocatalyst (i.e., the electrode) itself may undergo oxidation and reduction (redox) reactions, which results in variations in the resistance and potential of the electrodes. Recent advances in operando spectroscopy techniques, such as ambient pressure X-ray photoelectron spectroscopy (AP-XPS), *in situ* X-ray diffraction (XRD), and high temperature transmission electron microscopy (HT-TEM), have the potential to reveal nano-scale views of the electrocatalyst²²⁻²⁴. However, unequivocal elucidation has not occurred because of the unrealistic measurement and specimen conditions required for operando spectroscopy²⁵. Therefore, a better *in situ* characterization technique employed under operating conditions with the real composite electrodes is needed.

Herein, we demonstrate a novel *in situ* technique using electrochemical measurements that enables the characterization of the active surface sites on a yttria-stabilized zirconia (YSZ)-supported Ni catalyst during



the partial oxidation of methane under real operating conditions. Ni is one of the most important electrocatalysts utilized in the production of hydrogen from biomass and in fuel reforming such as steam reforming and partial oxidation of methane^{26–28}. During the partial oxidation of methane, oscillations in the reaction rate, temperature, and gas composition have been observed on Ni catalysts^{29–33}. In general, it is thought that the oscillatory behavior originates from the repetitive cycles of the oxidation and reduction of catalysts^{23,34,35}. The SOCs consisted of Ni-YSZ | YSZ | La_{0.8}Sr_{0.2}MnO₃ (LSM)-YSZ with real composite electrodes and were adopted to elucidate the role of the chemical states contributing to the oscillation behavior during the partial oxidation of methane. *In situ* electrochemical analysis using time-variant potential and impedance measurements enabled us to determine the real-time variation of the active sites of the electrochemical and redox reactions. Our results provide an in-depth understanding of the nano-scale redox behavior of a Ni electrocatalyst and a rational design rule for redox stable Ni catalysts.

Results

A SOC composed of Ni-YSZ | YSZ | LSM-YSZ was employed to characterize the redox behavior of nickel with a dual chamber configuration, as illustrated in Fig. 1a. The Ni-YSZ anode microstructure of the SOC is shown in Fig. 1b and 1c. The details of the fabrication processes and measurement conditions are described in the Methods section. The oscillation of open circuit voltage (OCV) in SEP measurements was induced at 800 °C under stoichiometric conditions for partial oxidation with a methane-to-oxygen ratio (CH₄/O₂) of 2. The OCV fluctuated with a period of 30 s, as shown in Fig. 2a. This oscillation period is dependent on the total flow rate, temperature, and gas composition^{30,31}. The potential for the SOC, which is based on an oxygen ion-conducting electrolyte, can be developed using the concentration gradient of oxygen ions between the cathode and anode according to the Nernst equation:

$$E = \frac{RT}{4F} \ln \frac{a_{\text{O}_2}^{\text{cathode}}}{a_{\text{O}_2}^{\text{anode}}}$$

where F is the Faradaic constant, a_{O_2} is the activity of the oxygen ions at the electrode, which is approximated as the oxygen partial pressure, and R and T are the gas constant and temperature, respectively. The concentration of the oxygen ions at the cathode is considered to be constant because a continuously supplied air-flow maintains a constant partial pressure of oxygen. Therefore, it can be inferred that the cyclic oxidation and reduction of nickel at the anode results in the oscillation of OCV. When nickel is oxidized, the potential of the anode increases upon electron loss, and

the OCV decreases; the OCV increases if the nickel is reduced again. Using the cyclic variation of the OCV, the oscillation of the oxygen partial pressure at the anode can be calculated as shown in Fig. 2b.

Electrochemical impedance spectroscopy (EIS) during cell operation also showed the oscillatory behavior, as depicted in Fig. 2c. It is improper to use the typical Nyquist plot, which plots the impedance (Z) as a function of the frequency under constant DC bias, to characterize the polarization involved in an oscillating system. Therefore, we measured the impedance as a function of time under a zero DC bias at a constant frequency of 5 kHz, in which the relaxation time is sufficiently short to prevent overlapping of the data points. The zero bias condition in which no external static potential is applied (i.e., no DC current flow) is set in impedance spectroscopies with a small AC signal to maintain thermal equilibrium of the cell with its surroundings (i.e., gas or liquid medium). This enables gas or liquid reactants to be in equilibrium states during a reaction. In this respect, the impedance responses to small AC signals are attributed to chemical/electrochemical reactions at the cell³⁶. An equivalent circuit for the Ni-YSZ | YSZ | LSM-YSZ cell adapted from the model suggested by Barfod *et al.* is proposed, as shown in Fig. S1 (Supplementary Information). This circuit contains five parallel capacitors (C) and resistors (R) with a serial contribution³⁷. Each process in electrodes was determined by variations of experimental conditions as proved in earlier studies³⁸. They demonstrated that the 1 kHz high-frequency sub arc represents charge transfer between Ni and YSZ at TPBs of the anode. Because we are only interested in oxygen transport between Ni and YSZ, the impedance response was measured under a constant frequency of 5 kHz, similar to the summit frequency of the sub arc reported by Barfod *et al.* EIS spectra under H₂ and POX condition (CH₄ + O₂) showed the polarization variation due to the change of fuel gas as plotted in Fig. S2a (Supplementary Information). Each spectrum appeared to consist of a large high-frequency arc and a small low-frequency arc. The high-frequency arc was larger under POX condition than H₂, suggesting that this arc is associated with the anodic process dominantly. Bode plots also exhibited that the frequency of maximum phase shift around 1 kHz slightly changed upon change of fuel gas as shown in Fig. S2b (Supplementary Information). It is therefore reasonable that the interfacial resistance and capacitance determined from the high frequency impedance arc at 5 kHz represent charge transfer between Ni and YSZ near TPBs. The impedance oscillated with a characteristic periodicity of 30 s, which is similar to that observed in the OCV oscillation. Two distinct regimes can be identified by the magnitudes of the real (Z_{real}) and imaginary (Z_{imag}) components of the impedance, as shown in Fig. 2d. The first regime exhibited a metallic

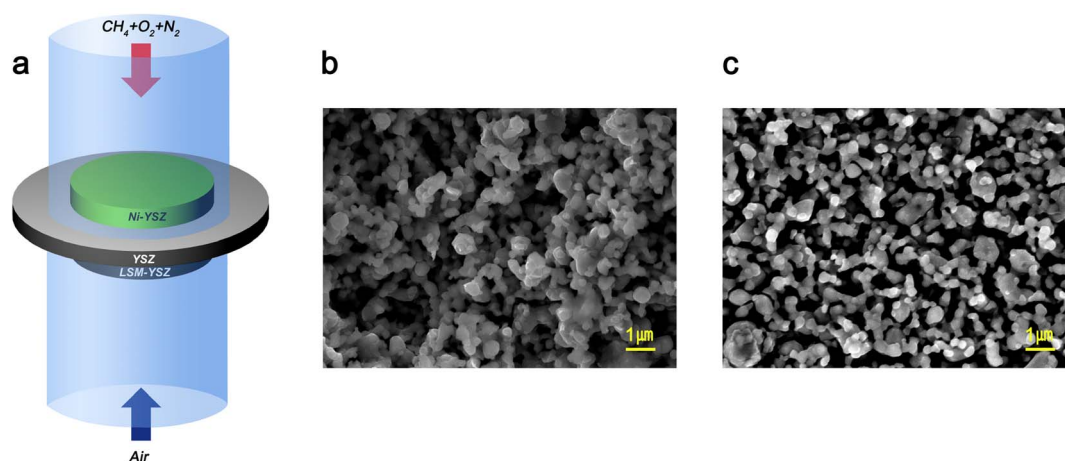


Figure 1 | SOC employed in this work. (a) Schematic illustration of measurement configuration for electrochemical characterizations. And SEM images of the Ni-YSZ anode after electrochemical characterizations. (b) Cross-sectional image and (c) plain image of the Ni-YSZ surfaces.

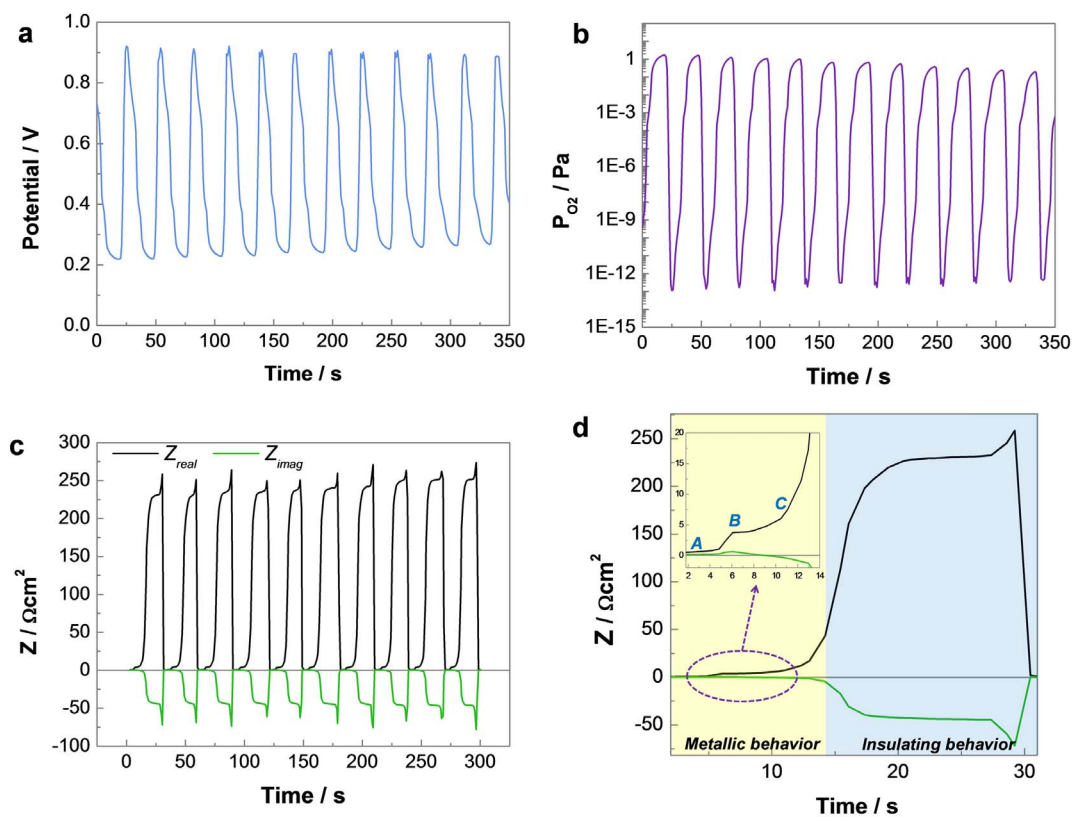


Figure 2 | Oscillatory behavior with time. (a) OCV oscillation under a methane-to-oxygen atmosphere ratio (CH_4/O_2) of 2, which is the stoichiometric condition for the partial oxidation of methane. (b) Equilibrium oxygen partial pressure oscillation at the anode calculated from the Nernst equation. (c) The oscillation of impedance as a function of time. (d) Inset image shows the detailed variation of the impedance at the initial stage in the metallic regime.

behavior characterized by small Z_{real} and Z_{imag} values. The first regime was replaced by an insulating regime at 14 s, in which large Z_{real} and Z_{imag} values were observed. The insulating behavior results from a percolation failure in the anode. When the metallic portion (i.e., Ni) decreases below a critical point because of the oxidation, the conductivity of the anode drops abruptly³⁹. Therefore, the resistance (Z_{real}) increases rapidly, and the electrons can accumulate at the interface between the oxide and metallic phase, inducing large Z_{imag} or capacitance.

Discussion

We adopted the assumptions and expression for the interfacial polarization from continuum model^{36,38,40}. Because oxygen ion transport toward 3PBs is characterized by high frequency polarization, interfacial resistance and capacitance are expressed exactly as the polarization between electrode and electrolyte under steady-state conditions of oxygen ion transport. Interfacial capacitance is dielectric capacitance due to charge transfer between the ion conductor and electron conductor, i.e., YSZ electrolyte and Ni electrode⁴⁰. Interfacial resistance is inversely proportional to equilibrium oxygen partial pressure and electrochemical charge transfer rate constant (k), which is defined in the Chang-Jaffe boundary conditions^{40,41}. In this case, Z_{imag} can be expressed as a function of the equilibrium concentration of oxygen ions and the electrochemical charge transfer rate constant, as well as the resistance and capacitance. To separate the anodic polarization from the total polarization during the oscillation, Z_{imag} is differentiated with time. The derivative of the impedance as a function of time can be approximated to the anodic polarization variations as a function of time because the partial pressure at the cathode remains constant and the cathodic polarization is assumed to be constant over time. Then, we obtained the anodic

electrochemical charge transfer rate constant (k), which can be regarded as the oxygen transport rate constant at anode. The detailed mathematical derivations are described in the Supplementary Information.

The electrochemical charge transfer rate constant (k) was plotted (Fig. 3a) as a function of time as well as Z_{real} . Rate constant variation was only observed in the metallic region (from A through B to C) with a periodicity of 30 s, which is similar to that of impedance. Points A, B, and C distinguished the metallic region. At point B, constant polarization resistance and maximum electrochemical reaction rate were observed, indicating that the nickel is fully reduced at this stage. From B to C, reaction rate decreased drastically while polarization resistance increased. This phenomenon is because a decrease in electrical conduction retards electrochemical charge transfer at this stage. For this reason, selective oxidation of Ni at two phase boundaries (2PBs) at the precedent stage only raised resistance. Further oxidation led to a break in percolation conduction, which gave rise to the drastic decrease in electrochemical reaction rate and increases in both resistance and capacitance. From the insulating region to A, electrochemical charge transfer was facilitated first and recovery of percolation conduction followed. Gas chromatography (GC) results of the outgas collected during oscillation support an active partial oxidation (POX) reaction even in the insulating region. Substantial amounts of H_2 and CO were observed in all sub-stages, as shown in Fig. 4a. It is possible that the concentration variation of H_2 and CO in outgas is related to the state of Ni catalysts. The concentrations of CH_4 and O_2 simultaneously varied, indicating consumption of O_2 by POX. The maximum relative concentration of H_2 to CO was observed at point B, while the minimum ratio of H_2 to CO was detected at the insulating region as shown in Fig. 4b. These phenomena can reflect that H_2 is consumed upon the reduction of

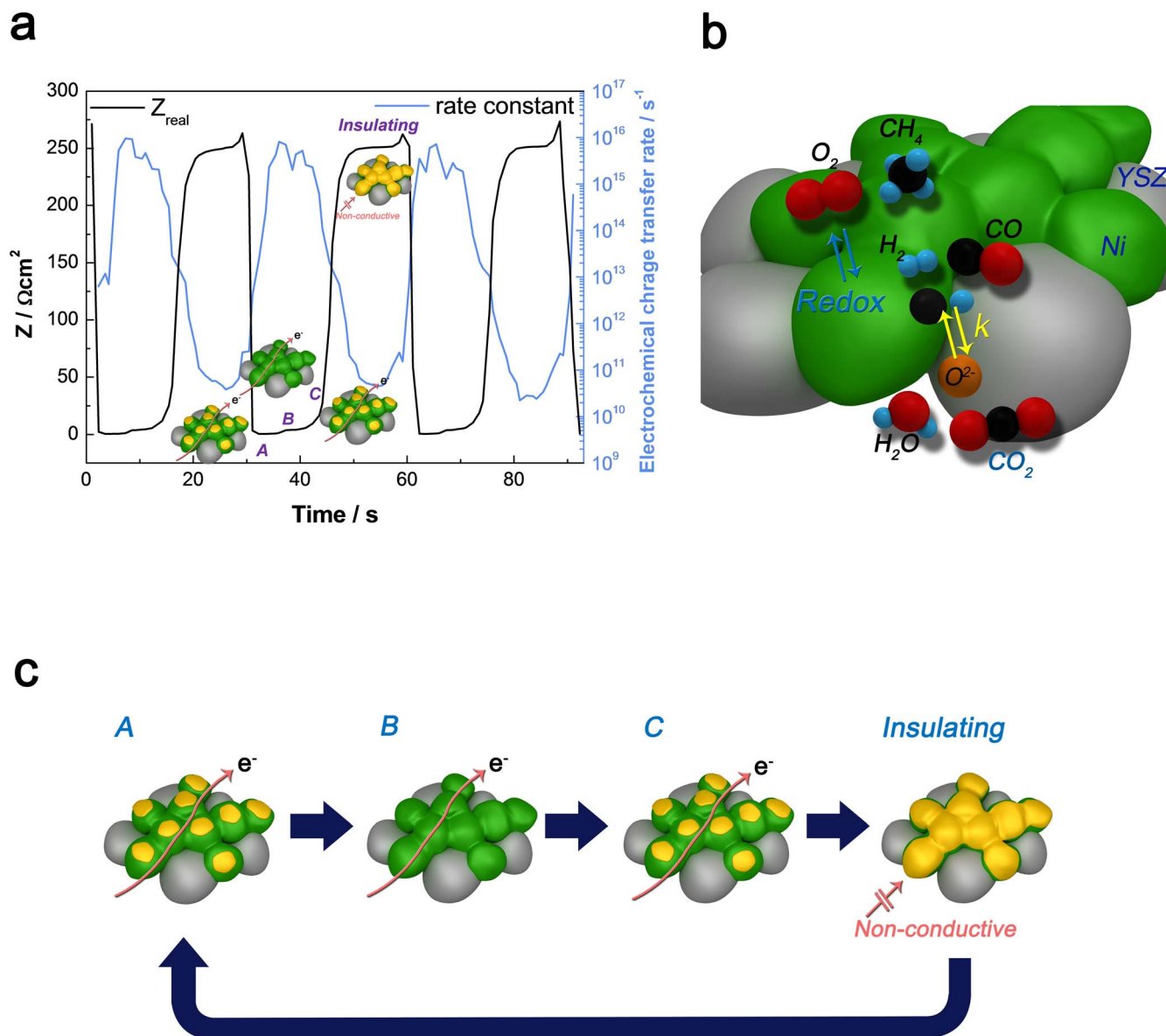


Figure 3 | Oscillation of the electrochemical charge transfer rate constant at anode as a function of time. (a) Rate constant oscillation was calculated from Z_{imag} and simultaneously varying Z_{real} was also plotted. (b) Possible reactions occurring at anode include chemical reactions such as redox reactions, dissociative adsorption, diffusion of adsorbates toward 3PBs, partial oxidation of methane (POX), and electrochemical reactions that generate oxygen ion flux by which H_2 and CO are consumed at 3PBs (i.e., interface of Ni (green), YSZ (grey), and gas), while nickel oxidation occurs at 2PBs. (c) Schematic illustration of redox procedures during the oscillation.

NiO from insulating to *B* region accompanying formation of H_2O^{42} . CO_2 generation serves as a descriptor for the electrochemical conversion of CO by oxygen ions because O_2 is used in POX. The relative ratio of CO_2 to CO , defined as electrochemical conversion rate, exhibited a maximum value at point *B*, which decreased drastically at point *C* and began increasing at the insulating region as shown in Fig. 4c. This behavior is consistent with variation in the electrochemical charge transfer rate constant calculated from EIS and SEP results. These characteristic variations in the rate constant combined with the impedance provide a clue for understanding the surface states of Ni subjected to the repeated redox reaction. In our SOC, the chemical and electrochemical reactions simultaneously occur, as shown in Fig. 3b. The oxygen current through the cell is developed by the electrochemical reactions at electrodes, which includes both the reduction of the oxygen gas to oxygen ions at the cathode and the oxidation of $\text{H}_2 + \text{CO}$ by the oxygen ions at the anode. The electrochemical reaction primarily occurs at the 3PBs of the nickel, oxide

support (YSZ), and gas. The partial oxidation of methane produces syngas (i.e., $\text{H}_2 + \text{CO}$) as methane undergoes a chemical reaction with oxygen at the anode. The dissociative adsorptions of both methane and oxygen occur on the surface of nickel, which acts a heterogeneous catalyst. Nickel can undergo a transient oxidation by the adsorbed oxygen. As the partial oxidation of methane proceeds, the local atmosphere is shifted toward a reducing environment due to the increased partial pressure of $\text{H}_2 + \text{CO}$, under which NiO is reduced again, accompanying the amount of active sites for electrochemical reactions. Therefore, the electrochemical reaction rate constant is determined by the metallic nickel content at the 3PBs. In contrast, the oxidation of nickel at two-phase boundaries (2PBs) composed of nickel and gas will affect the electronic conduction through the electrodes because the 2PBs are inactive sites for the electrochemical reactions.

Based on these considerations, the oscillation of the rate constant can be explained in terms of the variation in the metallic nickel at the

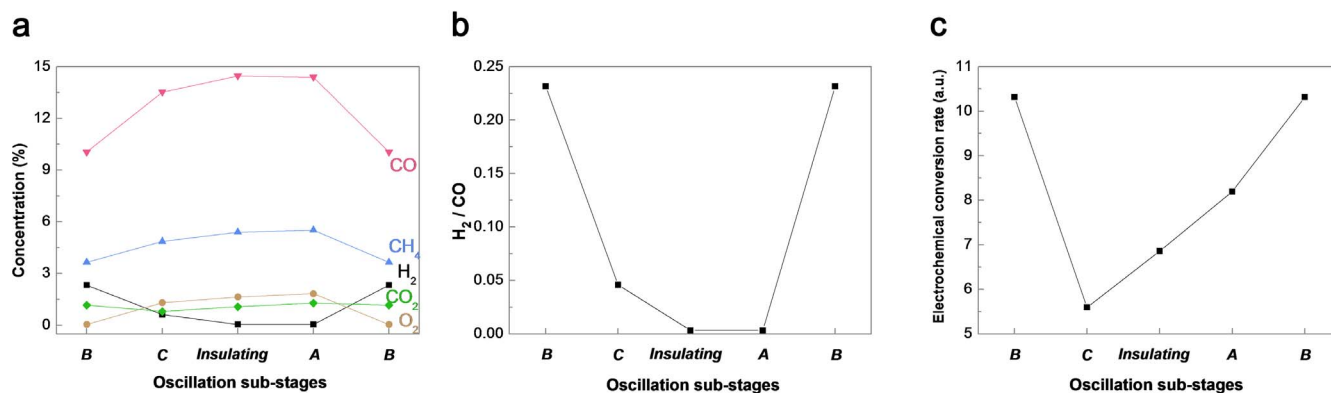


Figure 4 | Composition of outgas during oscillation exhibited periodic oscillation depending on reaction sub-stages. Gas chromatography (GC) results of outgas during oscillation characterized by sub-stages. (a) Relative outgas concentration during oscillation, (b) relative ratio of H₂ to CO and (c) electrochemical conversion rate, defined as relative ratio of CO₂ to CO.

2PBs, which is schematically illustrated in Fig. 3c. From point A to B, which is characterized by the recovery of the metallic behavior, the constant reaction rate is indicative of the dormancy of the electrochemical reactions. However, the chemical reaction (i.e., reduction of nickel) is allowed. From the B to C, the maximum electrochemical reaction rate indicates that nickel is fully reduced. The subsequent decrease in the rate constant indicates the initiation of the Ni re-oxidation (yellow phase) manifested by the increased anodic resistance (Fig. 2d inset). The decrease in the electrochemical reaction in this region may be attributed to sluggish electron conduction upon oxidation at the 2PBs because the Z_{imag} , which is strongly dependent on the capacitance and related to the electron transfer at the surface, remains constant. Further oxidation of the nickel prevents conduction of electrons. When the anode is sufficiently oxidized, resulting in an insulating behavior that is characterized by a drastic increase in both Z_{imag} and Z_{real} , the partial derivative of the reaction rate constant becomes nearly zero (from the C to insulating regime). This result indicates that the nickel at the 3PBs remains in a metallic state, even though the anode has a low electronic conductivity due to the percolation failure.

We analyzed the surfaces of the anode that are exposed to two different partial oxidation atmospheres in which methane-to-oxygen ratio was either 2 (the stoichiometric condition for partial oxidation of methane, i.e., active POX condition) or 3.33 (inactive POX condition) using conductive (c)-AFM to verify our proposed model. Fig. S3 (Supplementary Information) shows the OCV variation of the cell under the inactive POX condition (CH₄/O₂ = 3.3). The cell exhibited no oscillations in OCV, and a stable OCV of 0.95 V was measured (denoted as the *inactive POX cell*). The development of a stable and high OCV indicates that no repeated redox reaction occurred in the anode. However, a higher oxygen partial pressure gradient between the anode and cathode sets up under the oxygen deficient condition. The c-AFM analysis enabled us to distinguish the conducting phase from the non-conducting phase in the anode, in contrast with the typical topographical image (Fig. S4 in Supplementary Information). The conducting region was marked with a brighter color in Fig. 5. Detailed image conversion processes are shown in Fig. S5 and Table S1 in Supplementary Information. The area fraction (%) of the conducting region was higher for the anode that underwent oscillation (denoted as the *active POX cell*, i.e., the cell exposed to the stoichi-

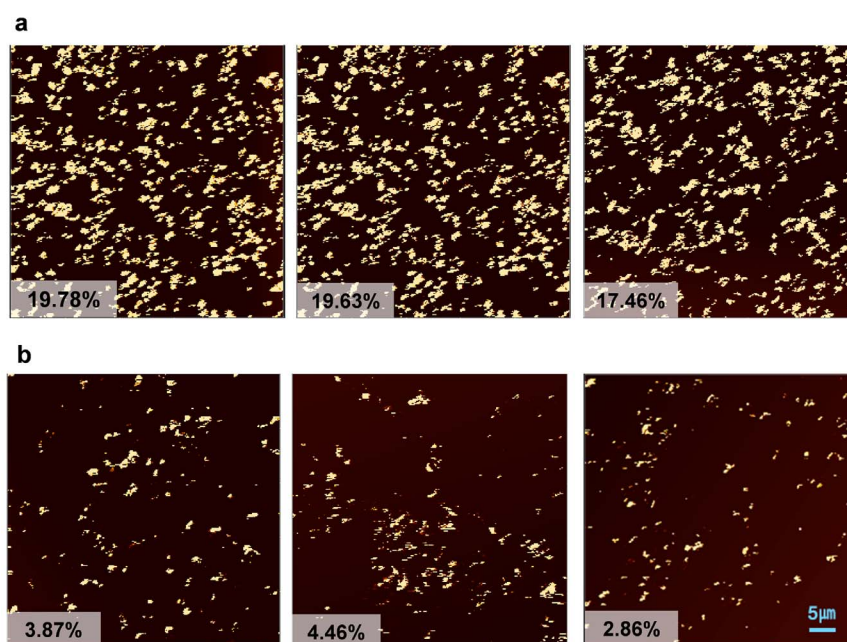


Figure 5 | Results of conductive-AFM surface analyses. Surface images of (a) the *inactive POX cell*, and (b) *active POX cell*, were obtained by c-AFM. The conducting regions are represented as bright areas in the images and can be regarded as metallic Ni.



ometric condition of $\text{CH}_4/\text{O}_2 = 2$). The average conductive area was $18.96 \pm 1.06\%$ within the scanned anode area of the *active POX cell*. However, only $3.73 \pm 0.66\%$ accounted for the conducting phase in the anode of the *inactive POX cell*, even though the oxygen partial pressure was lower in the *inactive POX cell*. It should be noted that the conductive area defined by c-AFM represents the region where the outermost surface remains a metallic nickel because the bias voltage is applied to the top of the surface. The higher surface area fraction of the conducting phase is indicative of less surface oxidation in the Ni-YSZ anode that is exposed to the stoichiometric condition in which methane is partially oxidized to produce $\text{H}_2 + \text{CO}$. At the 3PBs where the electrochemical oxidation of $\text{H}_2 + \text{CO}$ is active, the removal of $\text{H}_2 + \text{CO}$ from the Ni surfaces near the 3PBs allows continuous partial oxidation of methane, which consumes the adsorbed oxygen such that nickel remains in the metallic state without oxidation. However, at the 2PBs where the electrochemical oxidation is inactive, the consumption of $\text{H}_2 + \text{CO}$ is slow, and the continuous partial oxidation of methane is not allowed, resulting in the oxidation of nickel at the 2PBs by the adsorbed oxygen. However, the partial oxidation of methane does not actively occur because the oxygen is unable to readily oxidize CH_4 over the anode exposed to the oxygen deficient atmosphere (i.e., the *inactive POX cell*). This eliminates the difference between the 2PBs and 3PBs, and the Ni is oxidized regardless of the surface site types. Therefore, the entire surface of the Ni is oxidized, as indicated by a lower surface area fraction of the conducting phase compared with the anode of the *active POX cell* in which the electrochemically active 3PB sites are reduced by the product ($\text{H}_2 + \text{CO}$) of the catalytic partial oxidation.

Scanning transmission electron microscope (STEM)-electron energy-loss spectroscopy (EELS) analysis was performed on cross-sectioned anodes from both the *active POX* and *inactive POX cells* using a focus ion beam (FIB) to provide clear evidence of the selective oxidation (Fig. 6). EELS mapping images were reconstructed for colored visualization and raw images of chemical maps are available in Fig. S6 (Supplementary Information). The chemical EELS maps of the Ni, Zr, and O were constructed to compare the oxidation state of Ni at the surface of an isolated nickel grain (i.e., 2PBs) and the interfaces between Ni and YSZ (i.e., 3PBs). In the *inactive POX cell*, the nickel oxide layers were clearly visible at both the 2PBs and 3PBs, as shown in Fig. 6a and 6b. The peaks for the O K-edge and Ni L-edge co-existed at the interface of Ni and YSZ, as well as on the surface of Ni. The thickness of the oxide layer surrounding the 2PBs and 3PBs was approximately 50–70 nm. In contrast, the non-uniform distribution of the nickel oxide layer was observed in the *active POX cell* and only detected at the 2PBs, as shown in Fig. 6c. The thickness of the oxide was approximately 50–70 nm, which is similar to that in the *inactive POX cell*. The O K-edge peak obtained from the outermost layer of Ni interfaced with YSZ was invisible (Fig. 6d), which indicated a lack of oxidation of the nickel at the 3PBs under active operating conditions for the partial oxidation of methane.

Our results suggest that the redox reactions of the electrodes occur predominantly at the 2PBs, whereas the electrochemical reactions are active at the 3PBs that remain in a metallic state. Based on these results, it can be inferred that a stable OCV can develop in a cell that has a stoichiometric atmosphere when the 3PBs are extensively enlarged with respect to the 2PBs. An increase in the 3PBs over the

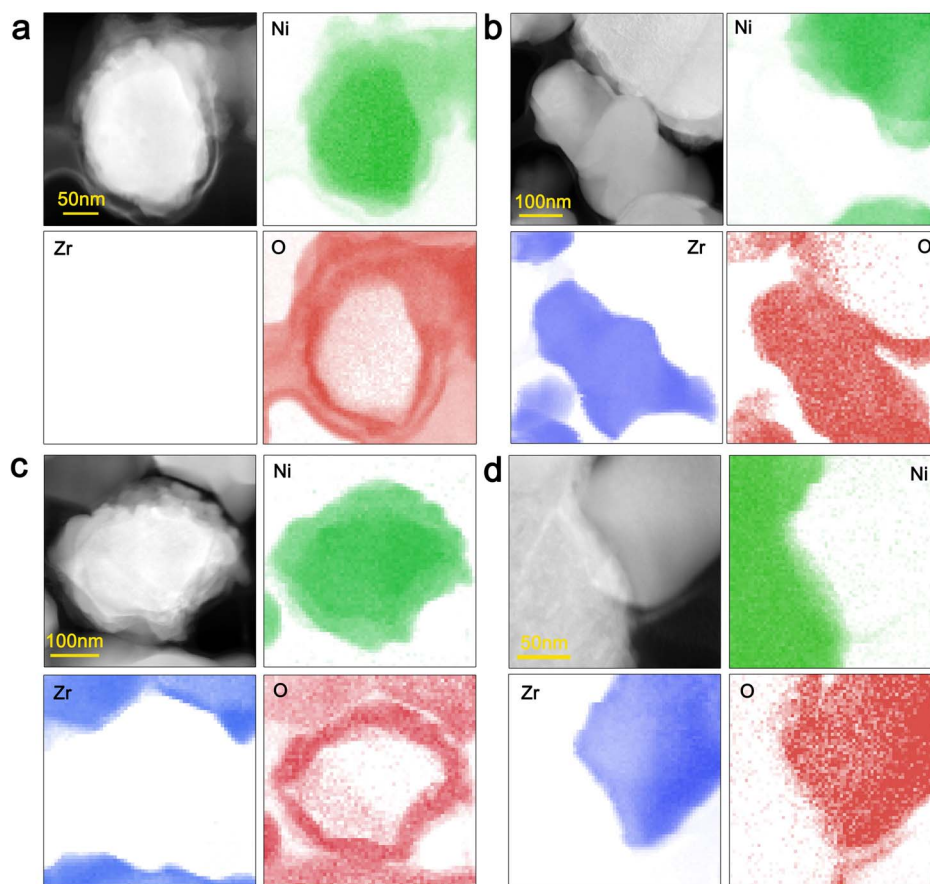


Figure 6 | STEM-EELS images of the *inactive POX* and *active POX cells*. EELS chemical maps of Ni, O, and Zr obtained from the Ni L-edge, O K-edge, and Zr M-edge, respectively, are shown with the corresponding STEM images. The EELS chemical maps were reconstructed for colored visualization and the raw images of the chemical maps are available in the Supplementary Information (Figure S6). (a) EELS chemical maps and STEM images of a 2PB in the *inactive POX cell*; (b) a 2PB in the *active POX cell*; (c) a 3PB in the *active POX cell*; and (d) a 3PB in the *active POX cell*.



2PBs can form oxidation-resistant surface sites, resulting in a constant partial pressure gradient of oxygen without OCV oscillation. We prepared the Ni-YSZ anodes with different relative ratios of 3PBs/2PBs by controlling the Ni particle size and Ni/YSZ composition, whereas the anode thickness remained constant. The two-dimensional ratio of 3PBs/2PBs was quantified by *c*-AFM based on the image analysis shown in Fig. S7 (Supplementary Information). The potential variations as a function of the 3PBs/2PBs ratio under the stoichiometric condition are depicted in Fig. 7. The cell that was based on the anode with the highest 3PBs/2PBs ratio (1.08 m^{-1}) exhibited stable and high OCV, as shown in Fig. 7a. However, the other cells exhibited oscillating (0.99 m^{-1}) and low OCV (0.78 m^{-1}) (Fig. 7b and 7c) due to the increased degree of nickel oxidation. Once the site density of the 3PBs reaches a critical value, continuous and stable partial oxidation is permitted, preventing the oxidation of the Ni catalysts. Below the critical value, the oxidation of nickel readily occurs predominantly at the 2PBs, and the selective oxidation-reduction induces the potential oscillation. If the site density of the 3PBs is much lower than that of the cell with the OCV oscillation, the oxidation reaction dominates over the entire nickel surface, and the potential difference between the cathode and the anode does not develop.

In this study, the oscillation behavior of a Ni-YSZ catalyst system in a SOC was characterized via *in situ* electrochemical analysis. The repeated oxidation and reduction cycles of nickel during the partial oxidation of methane provide an ideal system for in-depth elucidation of the Ni oxidation as a function of surface site types. The variation in the anodic electrochemical rate constant was determined by a non-stationary impedance analysis with a constant frequency and a time-variant OCV measurement. Based on the results from these analyses, we proposed a surface oxidation mechanism for Ni. The electrochemical charge transfer rate constant remained constant even when the anode underwent maximum oxidation, which implied that the oxidation of nickel only influenced the increase in the resistance and not the electrochemical reaction. Our observations indicated that nickel at the 3PBs, where the electrochemical reactions are active, remains in the metallic state and that the oxidation predominantly occurs at the 2PBs. The *ex situ* surface analyses by *c*-AFM and STEM-EELS provided visible evidence for the selective oxidation at the 2PBs. Further experiments with various surface site ratios clearly confirmed the control of the potential variation by adjusting the relative 3PBs/2PBs ratio when the partial oxidation of methane is active. Our results allowed us to propose a new design strategy for preparing novel supported catalysts with both excellent electrocatalytic activity and redox stability. These catalysts can be designed by extensively enlarging the 3PBs using nano-grained structure and/or selectively doping the surface of the 2PBs to hinder the oxidation.

Methods

A SOC that consisted of Ni-YSZ | YSZ | LSM-YSZ was fabricated for electrochemical characterization. A YSZ (TZ8Y, Tosoh Co., Tokyo, Japan) pellet with a diameter of 20 mm was prepared by uni-axial pressing, followed by sintering at 1500°C for 10 h, and served as an oxygen ion conducting solid electrolyte. The Ni-YSZ working electrode (anode) was deposited by a screen-printing technique using a paste of NiO-YSZ composite powders (NiO: YSZ = 66:34 wt%, Fuel Cell Materials Co., Lewis Center, OH, USA) dispersed in α -terpinol (Sigma-Aldrich Co., St. Louis, MO, USA). The paste was smeared on the YSZ pellet and fired at 1200°C for 2 h. The LSM-YSZ counter electrode (LSM: YSZ = 70:30 wt%) was fabricated in a similar fashion using a paste of LSM (Fuel Cell Materials Co., Lewis Center, OH, USA) and YSZ powders, followed by sintering at 900°C for 4 h. Prior to the electrochemical measurement, NiO was reduced to nickel under an atmosphere containing 4 vol% H_2 -Ar.

The potential oscillations were monitored by measuring the open circuit voltage (OCV) for the cells with a potentiostat (Solartron 1287A, Durham, UK). Electrochemical impedance spectroscopy was also conducted in the same configuration with a potentiostat and frequency analyzer (Solartron 1252, Durham, UK). The Ni-YSZ electrode was exposed to a flow containing a CH_4 and O_2 mixture (N_2 balanced, $\text{CH}_4:\text{O}_2 = 2:1$ or $3.33:1$) at 800°C , and artificial air ($\text{O}_2:\text{N}_2 = 21:79$) was fed to the LSM-YSZ electrode. Impedance spectra with a constant frequency of 5 kHz and AC current of 1 mA without DC bias were obtained as a function of time. After the electrochemical investigations, the cells were cooled to room temperature under Ar purging for *ex situ* surface characterization. The outgas composition variation was

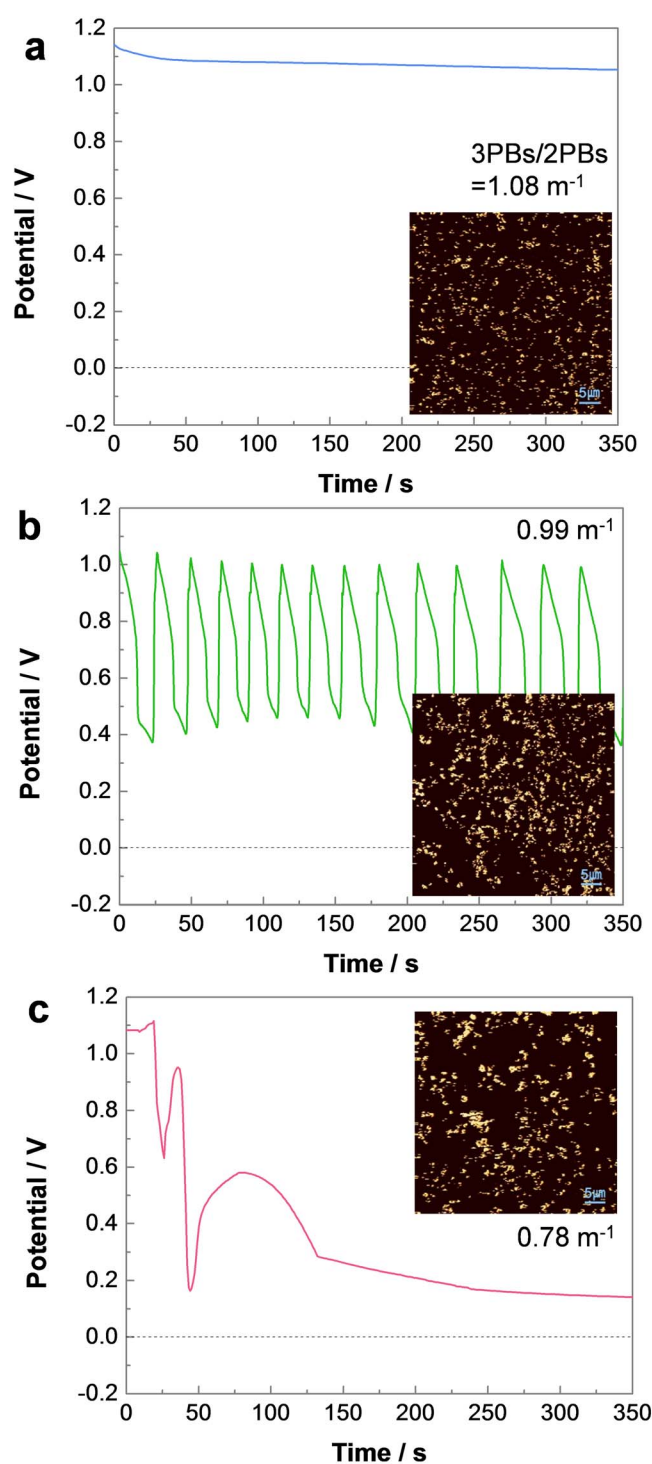


Figure 7 | Potential variations in cells with different 3PBs/2PBs ratios under the stoichiometric conditions for partial oxidation as a function of time. The cells had different 3PBs/2PBs ratios, and the thickness of the Ni-YSZ composite remained constant. The 3PBs/2PBs ratio of each cell was determined by *c*-AFM surface analysis, and the corresponding surface images are shown in the inset. (a) The anode that had the highest 3PBs/2PBs ratio (1.08 m^{-1}) exhibited stable OCV. (b) The anode that had an intermediate 3PBs/2PBs ratio (0.99 m^{-1}) exhibited oscillation of the OCV. (c) The anode that had the lowest 3PBs/2PBs ratio (0.78 m^{-1}) did not exhibit a stable OCV.

analyzed by a gas chromatography (GC) system (Acme 2200, Younglin, Seoul, Republic of Korea) equipped with Molesieve 5A, Porapak N columns and a thermal conductivity detector (TCD). The TCD signals were calibrated with CH_4 , H_2 , CO , CO_2 , and N_2 standard gasses in Ar balance gas and air. Conductive atomic force



microscopy (c-AFM, SPA400, SII, Tokyo, Japan) was conducted in a scan area of $50\ \mu\text{m} \times 50\ \mu\text{m}$ with a DC bias of 7 V. The conductive area was identified by an image analysis program (ImageJ, National Institutes of Health, Bethesda, MD, USA). Scanning transmission electron microscope (STEM)-electron energy-loss spectroscopy (EELS) analysis (JEM-ARM200F, JEOL, Tokyo, Japan) was performed on the Ni-YSZ anodes of both the *active POX* and *inactive POX cells*. Energy-loss spectra at approximately 854.5–903.5 eV, 533.9–582.9 eV, and 202.7–253.1 eV were assigned to the Ni L-edge, O K-edge, and Zr M-edge, respectively, with the calibration of the C K-edge at 284 eV.

The samples with different 3PBs/2PBs ratios were prepared using three different Ni-YSZ composite powders with a different composition and specific surface area. The commercial NiO-YSZ powders (Product numbers 164-124, 279-01, 5A055, Fuel Cell Materials Co., Lewis Center, OH, USA) were utilized to prepare the pastes, and the button cells were fabricated in the same manner as described above. The thickness of the NiO-YSZ anodes was maintained at $45\ \mu\text{m}$ after sintering at 1200°C , and all of the samples were pre-reduced in 4% H_2 -Ar balanced gas prior to the measurements at 800°C to ensure no critical difference in the microstructures between the samples. The 3PBs/2PBs ratio was determined by c-AFM using the fully reduced samples, which had been cooled down under 4% H_2 -Ar balanced gas. By performing image analysis of the images obtained by c-AFM with the *ImageJ* program, we calculated the conductive area and its perimeter, which corresponded to the 2PBs region and 3PBs length, respectively.

- Maroun, F., Ozanam, F., Magnussen, O. M. & Behm, R. J. The role of atomic ensembles in the reactivity of bimetallic electrocatalysts. *Science* **293**, 1811–1814 (2001).
- Atkinson, A. *et al.* Advanced anodes for high-temperature fuel cells. *Nat. Mater.* **3**, 17–27 (2004).
- Minh, N. Q. Ceramic fuel cells. *J. Am. Ceram. Soc.* **76**, 563–588 (1993).
- Wachsman, E. D. & Lee, K. T. Lowering the temperature of solid oxide fuel cells. *Science* **334**, 935–939 (2011).
- Hauch, A., Ebbesen, S. D., Jensen, S. H. & Mogensen, M. Highly efficient high temperature electrolysis. *J. Mater. Chem.* **18**, 2331–2340 (2008).
- Zhan, Z. *et al.* Syngas production by coelectrolysis of $\text{CO}_2/\text{H}_2\text{O}$: the basis for a renewable energy cycle. *Energy Fuels* **23**, 3089–3096 (2009).
- Bierschenk, D. M., Wilson, J. R. & Barnett, S. A. High efficiency electrical energy storage using a methane–oxygen solid oxide cell. *Energy Environ. Sci.* **4**, 944–951 (2011).
- Brandon, N. P., Skinner, S. & Steele, B. C. H. Recent advances in materials for fuel cells. *Annu. Rev. Mater. Res.* **33**, 183–213 (2003).
- Gorte, R. J. & Vohs, J. M. Catalysis in solid oxide fuel cells. *Annu. Rev. Chem. Biomol. Eng.* **2**, 1–22 (2010).
- Zhang, C. *et al.* Measuring fundamental properties in operating solid oxide electrochemical cells by using in situ X-ray photoelectron spectroscopy. *Nat. Mater.* **9**, 944–949 (2010).
- Wilson, J. R. *et al.* Three-dimensional reconstruction of a solid-oxide fuel-cell anode. *Nat. Mater.* **5**, 541–544 (2006).
- Chueh, W. C., Hao, Y., Jung, W. & Haile, S. M. High electrochemical activity of the oxide phase in model ceria–Pt and ceria–Ni composite anodes. *Nat. Mater.* **11**, 155–161 (2012).
- Tao, F. *et al.* Reaction-driven restructuring of Rh–Pd and Pt–Pd core-shell nanoparticles. *Science* **322**, 932–934 (2008).
- Tao, F. & Salmeron, M. In situ studies of chemistry and structure of materials in reactive environments. *Science* **331**, 171–174 (2011).
- Weppner, W. & Huggins, R. A. Electrochemical methods for determining kinetic properties of solids. *Annu. Rev. Mater. Sci.* **8**, 269–311 (1978).
- Yentekakis, I. V. & Vayenas, C. G. The effect of electrochemical oxygen pumping on the steady-state and oscillatory behavior of CO oxidation on polycrystalline Pt. *J. Catal.* **111**, 170–188 (1988).
- Yentekakis, I. V., Neophytides, S. & Vayenas, C. G. Solid electrolyte aided study of the mechanism of CO oxidation on polycrystalline platinum. *J. Catal.* **111**, 152–169 (1988).
- Vayenas, C. G. Catalytic and electrocatalytic reactions in solid oxide fuel cells. *J. Catal.* **28–30**, Part 2, 1521–1539 (1988).
- Hetrick, R. E. & Logothetis, E. M. Oscillations in the emf of solid-state electrochemical oxygen sensors. *Appl. Phys. Lett.* **34**, 117–119 (1979).
- Kokkofitis, C. & Stoukides, M. Rate and oxygen activity oscillations during propane oxidation on Pt/YSZ. *J. Catal.* **243**, 428–437 (2006).
- Cronin, J. S., Wilson, J. R. & Barnett, S. A. Impact of pore microstructure evolution on polarization resistance of Ni–Yttria-stabilized zirconia fuel cell anodes. *J. Power Sources* **196**, 2640–2643 (2011).
- Hansen, P. L. *et al.* Atom-resolved imaging of dynamic shape changes in supported copper nanocrystals. *Science* **295**, 2053–2055 (2002).
- Hendriksen, B. L. M. *et al.* The role of steps in surface catalysis and reaction oscillations. *Nature Chem.* **2**, 730–734 (2010).
- Butcher, D. R. *et al.* In situ oxidation study of Pt(110) and its interaction with CO. *J. Am. Chem. Soc.* **133**, 20319–20325 (2011).
- Topsoe, H. Developments in operando studies and in situ characterization of heterogeneous catalysts. *J. Catal.* **216**, 155–164 (2003).
- Besenbacher, F. *et al.* Design of a surface alloy catalyst for steam reforming. *Science* **279**, 1913–1915 (1998).
- Vernon, P. D. F., Green, M. L. H., Cheetham, A. K. & Ashcroft, A. T. Partial oxidation of methane to synthesis gas. *Catal. Lett.* **6**, 181–186 (1990).
- Huber, G. W., Shabaker, J. W. & Dumesic, J. A. Raney Ni–Sn catalyst for H_2 production from biomass-derived hydrocarbons. *Science* **300**, 2075–2077 (2003).
- Tulenin, Y. P., Sinev, M. Y., Savkin, V. V. & Korchak, V. N. Dynamic behaviour of Ni-containing catalysts during partial oxidation of methane to synthesis gas. *Catal. Today* **91–92**, 155–159 (2004).
- Zhang, X., Lee, C. S. M., Hayward, D. O. & Mingos, D. M. P. Oscillatory behaviour observed in the rate of oxidation of methane over metal catalysts. *Catal. Today* **105**, 283–294 (2005).
- Slinko, M. M., Korchak, V. N. & Peskov, N. V. Mathematical modelling of oscillatory behaviour during methane oxidation over Ni catalysts. *Appl. Catal. A-Gen.* **303**, 258–267 (2006).
- Ren, X. B., Li, H. Y. & Guo, X. Y. Monte Carlo simulation of the oscillatory behavior in partial oxidation of methane on nickel catalyst. *Surf. Sci.* **602**, 300–306 (2008).
- Bychkov, V. Y., Tyulenin, Y. P., Slinko, M. M. & Korchak, V. N. Nonlinear behaviour during methane and ethane oxidation over Ni, Co and Pd catalysts. *Surf. Sci.* **603**, 1680–1689 (2009).
- Slinko, M. M. Oscillating reactions in heterogeneous catalysis: What new information can be obtained about reaction mechanisms? *Catal. Today* **154**, 38–45 (2010).
- Wachsman, E. D. & Clites, T. L. Stable mixed-conducting bilayer membranes for direct conversion of methane to syngas. *J. Electrochem. Soc.* **149**, A242–A246 (2002).
- Macdonald, J. R. Theory of space-charge polarization and electrode-discharge effects. *J. Chem. Phys.* **58**, 4982–5001 (1973).
- Barfod, R. *et al.* Detailed characterization of anode-supported SOFCs by impedance spectroscopy. *J. Electrochem. Soc.* **154**, B371–B378 (2007).
- Macdonald, J. R. Simplified impedance/frequency-response results for intrinsically conducting solids and liquids. *J. Chem. Phys.* **61**, 3977–3996 (1974).
- Lee, J.-H. *et al.* Quantitative analysis of microstructure and its related electrical property of SOFC anode, Ni–YSZ cermet. *Solid State Ionics* **148**, 15–26 (2002).
- Jamnik, J. & Maier, J. Treatment of the impedance of mixed conductors equivalent circuit model and explicit approximate solutions. *J. Electrochem. Soc.* **146**, 4183–4188 (1999).
- Chang, H. & Jaffé, G. Polarization in electrolytic solutions. part I. theory. *J. Chem. Phys.* **20**, 1071–1077 (1952).
- Parravano, G. The reduction of nickel oxide by hydrogen. *J. Am. Chem. Soc.* **74**, 1194–1198 (1952).

Acknowledgments

This CRI work was supported by the National Research Foundation of Korea (NRF) grant funded by the Korea government (MEST) (No. 2012R1A3A2026417). The work was also partially supported by the institutional research program of the Korea Institute of Science and Technology (2E24691).

Author contributions

D.L. and J.M. conceived and designed the experiments. D.L. performed the electrochemistry experiments with the SOCs fabricated by D.L. and D.K. D.L. and J.K. conducted the c-AFM and STEM-EELS analyses. All of the authors contributed to the data analysis. D.L., J.K. and J.M. co-wrote the paper.

Additional information

Supplementary information accompanies this paper at <http://www.nature.com/scientificreports>

Competing financial interests: The authors declare no competing financial interests.

How to cite this article: Lee, D., Kim, D., Kim, J. & Moon, J. Characterizing nano-scale electrocatalysis during partial oxidation of methane. *Sci. Rep.* **4**, 3937; DOI:10.1038/srep03937 (2014).

This work is licensed under a Creative Commons Attribution-NonCommercial-NoDerivs 3.0 Unported license. To view a copy of this license, visit <http://creativecommons.org/licenses/by-nc-nd/3.0>